Interplay between nonequilibrium and non-Markovianity in controlling the entropic uncertainty bound

Abdul Basit ,[1,*] Hamad Ali ,[2] Gao Xianlong ,[3,†] Peng-Bo Li,[2] Gehad Sadiek ,[1,4] and Hichem Eleuch [1]

[1]*Department of Applied Physics and Astronomy, College of Sciences, University of Sharjah, Sharjah 27272, United Arab Emirates*
[2]*Ministry of Education Key Laboratory for Nonequilibrium Synthesis and Modulation of Condensed Matter, Shaanxi Province Key Laboratory of Quantum Information and Quantum Optoelectronic Devices, School of Physics, Xi'an Jiaotong University, Xi'an 710049, China*
[3]*Department of Physics, Zhejiang Normal University, Jinhua 321004, China*
[4]*Department of Physics, Ain Shams University, Cairo 11566, Egypt*

(Received 19 March 2024; accepted 6 June 2024; published 9 July 2024)

The entropic uncertainty relation imposes a limit on the accuracy of measurement outcomes of two conjugate observables, which can be reduced in the presence of quantum memory. We theoretically study the dynamical behaviors of the quantum-memory-assisted entropic uncertainty relation for a bipartite system under local nonequilibrium dephasing environments and a common nonequilibrium dephasing environment. Particularly, we study the influence of the competition between nonequilibrium and non-Markovianity in controlling the entropic uncertainty bound (EUB) in weak- and strong-coupling regimes. We find that the nonequilibrium nature renders a promising protocol to efficiently harness the EUB in both regimes without requiring any operations on the main system. Further, we reveal that the EUB can be significantly reduced in a common bath case compared to the case of local baths. Moreover, we elucidate the primary factor responsible for governing the dynamical behaviors of EUB by examining the interplay between quantum discord and the minimal missing information about the particle to be measured. In addition, we investigate the state preparation and measurement choice (SPMC) condition in both environmental setups with weak- and strong-coupling regimes. Remarkably, we show that the SPMC condition does not hold in the common environment scenario.

DOI: 10.1103/PhysRevA.110.012429

I. INTRODUCTION

The uncertainty relation is one of the crucial and remarkable aspects of quantum mechanics that distinguishes the quantum world from the classical one. It inevitably limits our knowledge to precisely predict the measurement outcomes of two conjugate observables simultaneously. In 1927, Heisenberg initially suggested the uncertainty relation corresponding to the momentum and position of a particle [1]. It is stated that measuring the position and momentum of a particle at the same time with high accuracy is impossible. This famous uncertainty relation was first formulated by Kennard [2] in the form of standard deviation, i.e., $\Delta x \Delta p \geqslant \hbar/2$. Later, Robertson [3] generalized this uncertainty relation for any two observables R_1 and R_2, as $\Delta R_1 \Delta R_2 \geqslant \frac{1}{2}|\langle\psi|[R_1, R_2]|\psi\rangle|$. However, this uncertainty bound is state dependent; therefore, it becomes meaningless when the state $|\psi\rangle$ exhibits the zero-expectation value for the commutator $[R_1, R_2]$ [4].

In the context of information theory, entropy was considered a preferable measure to quantify the uncertainty relation over the standard deviation approach [5,6]. The well-known and improved version of the entropic uncertainty relation (EUR) proved by Maassen and Uffink [7] may read as follows:

$$H(R_1) + H(R_2) \geqslant \log_2 \frac{c}{2}. \tag{1}$$

Here $H(\Pi) = -\sum_i p_i(\Pi) \log_2 p_i(\Pi)$ characterizes the Shannon entropy of the observables $\Pi \in (R_1, R_2)$, and $p_i(\Pi) = \langle\psi_i^{\Pi}|\varrho|\psi_i^{\Pi}\rangle$ denotes the probability of measuring observable Π on state ϱ with ith outcome. Furthermore, the complementarity of the observables R_1 and R_2 can be expressed as $c = \max_{j,k}\langle\psi_j^{R_1}|\psi_k^{R_2}\rangle$, where $|\psi_j^{R_1}\rangle$ and $|\psi_k^{R_2}\rangle$ are the eigenstates of R_1 and R_2, respectively. Notably, as c is related to the two observables, it explicitly reflects that the lower bound of the EUR does not depend on the given quantum state. Therefore, entropy is considered a more rigorous quantifier for formulating the uncertainty relation than the standard deviation.

Nevertheless, the uncertainty relations mentioned above do not apply when the measured particle is entangled with another particle, known as a quantum memory [8]. Berta *et al.* [9] addressed this gap by deriving a more generalized uncertainty relation called the quantum memory-assisted entropic uncertainty relation (QMA-EUR). This new uncertainty relation can be written as

$$S(R_1|B) + S(R_2|B) \geqslant \log_2 \frac{1}{c} + S(A|B). \tag{2}$$

Here, $S(A|B) = S(\varrho_{AB}) - S(\varrho_B)$ characterizes conditional von Neumann entropy, where $S(\varrho) = -\mathrm{tr}(\varrho \log_2 \varrho)$, and $S(\Pi|B)$ with $\Pi \in (R_1, R_2)$ represents the conditional entropy

*Contact author: abasitphy@gmail.com
†Contact author: gaoxl@zjnu.edu.cn

of the postmeasurement state $\varrho_{\Pi B} = \sum_i (|\psi_i^{\Pi}\rangle\langle\psi_i^{\Pi}| \otimes I)\varrho_{AB}(|\psi_i^{\Pi}\rangle\langle\psi_i^{\Pi}| \otimes I)$ after measurement performed by Π, where $|\psi_i^{\Pi}\rangle$ are the eigenstates of the observable Π, and I is the identity operator. The quantum correlations between A and B can result in a negative conditional entropy $S(A|B)$ [10], which, in turn, may suppress the lower bound given by Eq. (1). Consequently, the QMA-EUR can predict the measurement outcomes of the two observables R_1 and R_2 precisely (even with zero uncertainty) when A and B are maximally entangled. This uncertainty relation has been verified by various experiments [4,11–13] and has vital applications in quantum information science, including entanglement witness [14], quantum key distribution [15], quantum metrology [16], quantum teleportation [17], quantum batteries [18], and more as discussed in a recent review [19]. Moreover, QMA-EUR and its lower bound have been further studied recently in Refs. [20–23] for improvement.

All real quantum systems inevitably interact with environments, leading to the phenomenon of decoherence or dissipation, i.e., the rapid destruction of quantum correlations [24]. Hence, quantum correlations are fragile, and decoherence effects hinder their potential advantages in practical implementations. Particularly, in this scenario, several interesting questions arise: What are the consequences of environmental decoherence on QMA-EUR? Does the decoherence effect inevitably result in increased uncertainty due to the loss of quantum correlations? Is this uncertainty relation dependent only on quantum correlation in the presence of decoherence? To answer these questions, several studies have been conducted to unveil the effects of various decoherence models on the time evolution of QMA-EUR [25–31]. In these studies, the authors investigated different scenarios where either particle A or quantum memory B was exposed to a noisy environment or both locally experienced decoherent or dissipative environments. Furthermore, various environmental noise-controlled strategies have been employed to reduce uncertainty and its lower bound, including weak measurements, non-Markovianity, and filter operations [32–34]. Additionally, in all these studies, the environment was considered in equilibrium.

Recently, it has been reported that the nonequilibrium aspect of the dephasing environment offers a promising technique for controlling decoherence [35,36], quantum-to-classical transition [37], and quantum speed limit [38]. Moreover, nonequilibrium feature outperforms in quantum metrology [39], quantum parameter estimation [40], quantum state tomography [41], and quantum steering [42]. Additionally, nonequilibrium can also suppress non-Markovianity and disentanglement in two-qubit systems [43]. With these motivations in mind, we aim to investigate the dynamical behaviors of QMA-EUR under the nonequilibrium phase damping environments. For this purpose, we first study the entropic uncertainty bound (EUB) when the measured particle A and quantum memory B interact locally with their corresponding nonequilibrium dephasing environments. Both A and B are initially considered in the Bell-diagonal states. Specifically, we explore the effects of the nonequilibrium nature of the bath on the dynamics of EUB. Notably, in Refs. [27,33], the authors have revealed that non-Markovianity generally reduces the EUB while nonequilibrium suppresses the non-Markovian nature of the dynamical map [35–37]. In this scenario, one might intuitively think that nonequilibrium can increase EUB. However, this is not true; we show that the EUB can be diminished via the nonequilibrium feature in both weak- and strong-coupling regimes. Moreover, we shed light on the key factor that governs the dynamical behaviors of EUB by analyzing the interplay between quantum discord (QD) and the minimal missing information about the particle A to be measured.

Second, we set the same initial state and investigate the dynamics of the EUB when particle A and quantum memory B are coupled to a common nonequilibrium dephasing environment. Notably, it has been demonstrated in Refs. [44,45] that, depending on the initial state, the common bath setup provides a promising avenue for enhancing quantum correlations. In this context, one might think that the EUB will be reduced due to the amplification of quantum correlation rather than increase monotonically to a stable magnitude. However, we show that in the common bath case the EUB increases monotonically to a stationary value, which implies that quantum correlation is not the only factor that controls EUB. Interestingly, the rate at which the EUB tends to a steady-state value can be slowed down by the nonequilibrium aspect of the environment in both weak- and strong-coupling regimes. Moreover, we show that the maximum magnitude of EUB can be considerably lower in the common bath setup compared to the local baths in both weak- and strong-coupling. The reason behind these dynamical behaviors of the EUB is explored by examining the competition between quantum discord and the minimal missing information about the particle to be measured. In addition, we investigate the state preparation and measurement choice (SPMC) condition for the given initial state in both environmental setups and show that this condition cannot be satisfied under the common bath scenario. It indicates that the EUB is not tighter in the common bath; therefore, one may not compute entropic uncertainty (EU) directly from the joint entropy of the whole system.

The structure of the paper is outlined as follows: In Sec. II, the nonequilibrium dephasing models with their analytical solutions are presented. The dynamics of QMA-EUR for a bipartite system, locally subjected to the respective nonequilibrium dephasing environments, is given in Sec. III. Section IV is devoted to the dynamical behaviors of the QMA-EUR under the common nonequilibrium dephasing environment. In Sec. V, we explore the SPMC condition in both environmental setups in detail. The conclusion of our main findings is provided in Sec. VI.

II. NONEQUILIBRIUM DEPHASING MODELS AND THEIR SOLUTIONS

In this section, first, we assume that the measured particle, labeled as A, and the quantum memory, labeled B, are locally and independently subjected to nonequilibrium pure dephasing environments with nonstationary and non-Markovian statistical properties. In the second case, both A and B simultaneously interact with a common nonequilibrium pure phase damping environment. A complete analysis of these two distinct models is provided below.

A. The local nonequilibrium dephasing environments

Here we begin with the case where A and B are locally coupled to their respective nonequilibrium phase damping environments with non-Markovian and nonstationary features. To solve this model, we first consider the single-particle dynamics, which can be easily generalized to a two-qubit system via the Kraus operators representation approach [46–48].

Let us consider particle A, a two-level quantum system (qubit) that interacts with a nonequilibrium phase damping environment E, wherein the environmental effects induce random fluctuations in the intrinsic frequency of particle A, i.e., $\omega(t)=\omega_0+\delta(t)$ [49,50]. The transition frequency between $|1\rangle$ (excited) and $|0\rangle$ (ground) levels is denoted by ω_0, and the function $\delta(t)$ is associated to the environmental dichotomic noise, defined by the non-Markovian and nonstationary stochastic process. Furthermore, we suppose that energy of the system is constant, and stochastic fluctuations just bring pure dephasing in dynamics of particle A. In this context, the Hamiltonian of subsystem A and its corresponding environment can be expressed as [49–52]

$$H_A(t)=\frac{\hbar}{2}(\omega_0+\delta(t))\sigma_A^z, \tag{3}$$

where σ_A^z denotes the Pauli operator. The dynamics of the whole system is described by the Liouville master equation as

$$\frac{\partial}{\partial t}\rho(t;\delta(t))=-\frac{i}{\hbar}[H_A(t),\varrho(t;\delta(t))], \tag{4}$$

where the term $\varrho(t;\delta(t))$ indicates the state of the entire system which depends on the environmental noise $\delta(t)$.

For the time being, we are only interested in the dynamics of particle A. Therefore, its reduced state can be obtained by taking the statistical average over reservoir variables, i.e., $\varrho_A(t)=\langle\varrho(t;\delta(t))\rangle$. It is important to note that initially we assume an uncorrelated state between A and the corresponding phase damping environment. Thus, one can easily derive the reduced density matrix $\varrho_A(t)$ in the basis $\{|1\rangle,|0\rangle\}$ through the Kraus operators representation [41,43] as

$$\varrho_A(t)=\sum_{m=1}^{2}E_A^m(t)\,\varrho_A(0)\,E_A^{m\dagger}(t)$$
$$=\begin{pmatrix}\varrho^{11}(0) & \varrho^{10}(0)e^{-i\omega_0 t}\gamma_A{}^*(t)\\ \varrho^{01}(0)e^{i\omega_0 t}\gamma_A(t) & 1-\varrho^{11}(0)\end{pmatrix}, \tag{5}$$

where $\varrho_A(0)$ is the initial state of the particle A and $E_A^m(t)$ denote the Kraus operators for A, such that the condition $\sum_{m=1}^2 E_A^m(t)E_A^{m\dagger}(t)=I$ holds all the time. The Kraus operators for this model is given in Appendix A [see Eq. (A1)]. Furthermore, $\gamma_A(t)=\langle\exp[i\int_0^t\delta(\acute{t})d\acute{t}]\rangle$ describes the decoherence factor of particle A, and $\langle\ldots\rangle$ shows the statistical average over the environmental noise $\delta(t)$. The analytical expression for the decoherence factor of particle A can be derived as (for the details, see Ref. [37])

$$\gamma_A(t)=\mathcal{L}^{-1}[\Gamma_A(p)], \tag{6}$$

with

$$\Gamma_A(p)=\frac{p^2+(\beta+ia\upsilon)p+\beta(2\lambda+ia\upsilon)}{p^3+\beta p^2+(2\beta\lambda+\upsilon^2)p+\beta\upsilon^2}, \tag{7}$$

where $\mathcal{L}^{-1}$ defines the inverse Laplace transform with initial conditions $\gamma_A(0)=1$, $\frac{d}{dt}\gamma_A(0)=ia\upsilon$, and $\frac{d^2}{dt^2}\gamma_A(0)=-\upsilon^2$. The environmental noise $\delta(t)$ is characterized by a non-Markovian and nonstationary random telegraph process such that its amplitude randomly flips between $+\upsilon$ and $-\upsilon$ at an average rate of λ. The nonstationary and non-Markovian properties of this noisy process are described by the nonequilibrium parameter a and the memory kernel $K(t-\tau)=\beta e^{-\beta(t-\tau)}$ where β represents the damping rate, respectively. Unlike the equilibrium case, the decoherence factor $\gamma_A(t)$ is a complex time-dependent function because of the nonstationary aspect of the environmental noise. Notably, when $a=0$, the environment is in equilibrium, and $\gamma_A(t)$ becomes a stationary dichotomic noise; however, in other cases, the environment remains in nonequilibrium.

Now, we focus on the scenario where both the particle A and quantum memory B are under the local nonequilibrium dephasing environments. Therefore, by exploiting the Kraus operators representation method given in Refs. [41,43], we can straightforwardly derive the reduced density matrix for the bipartite state $\varrho_{AB}^L(t)$ in the basis $\{|1\rangle=|11\rangle,|2\rangle=|10\rangle,|3\rangle=|01\rangle,|4\rangle=|00\rangle\}$ as

$$\varrho_{AB}^L(t)=\sum_{n=1}^{4}F^n(t)\,\varrho_{AB}(0)\,F^{n\dagger}(t)$$
$$=\begin{pmatrix}\varrho^{11}(0) & \varrho^{12}(0)e^{-i\omega_0 t}\gamma_B{}^*(t) & \varrho^{13}(0)e^{-i\omega_0 t}\gamma_A{}^*(t) & \varrho^{14}(0)e^{-i2\omega_0 t}\gamma_A{}^*(t)\gamma_B{}^*(t)\\ \varrho^{21}(0)e^{i\omega_0 t}\gamma_B(t) & \varrho^{22}(0) & \varrho^{23}(0)\gamma_A{}^*(t)\gamma_B(t) & \varrho^{24}(0)e^{-i\omega_0 t}\gamma_A{}^*(t)\\ \varrho^{31}(0)e^{i\omega_0 t}\gamma_A(t) & \varrho^{32}(0)\gamma_A(t)\gamma_B{}^*(t) & \varrho^{33}(0) & \varrho^{34}(0)e^{-i\omega_0 t}\gamma_B{}^*(t)\\ \varrho^{41}(0)e^{i2\omega_0 t}\gamma_A(t)\gamma_B(t) & \varrho^{42}(0)e^{i\omega_0 t}\gamma_A(t) & \varrho^{43}(0)e^{i\omega_0 t}\gamma_B(t) & 1-[\varrho^{11}(0)+\varrho^{22}(0)+\varrho^{33}(0)]\end{pmatrix}, \tag{8}$$

where L stands for local baths, and $F^n(t)$ represent the Kraus operators for the bipartite system $\varrho_{AB}^L(t)$ [given in Eq. (A2)], where $\sum_{n=1}^4 F^n(t)F^{n\dagger}(t)=I$. The reduced density state $\varrho_{AB}^L(t)$ describes the time evolution of the two-qubit system where $\gamma_A(t)$ [$\gamma_B(t)$] is the dephasing factor of particle A (quantum memory B). Notably, the diagonal elements remain unchanged due to pure dephasing, and all the off-diagonal elements decay with time as $\varrho^L_{AB}(t)$ evolves. Moreover, we assume both qubits are initially in Bell-diagonal state $\varrho_{AB}(0)$, i.e.,

$$\varrho_{AB}(0) = \frac{1}{4}\left(I_{AB} + \sum_{j=1}^{3} \mu_j \sigma_A^j \otimes \sigma_B^j\right), \tag{9}$$

where I_{AB} represents the 4×4 identity matrix and $\sigma^j_{A(B)}$ is the jth component of the Pauli operator for $A(B)$. Furthermore, $\{\mu_j = \mu_j(0)\}$ represent the initial correlation parameters such that $-1 \leqslant \mu_j \leqslant 1$. The Bell-diagonal states lead to numerous applications; for example, Bell-diagonal states reveal the general form of the reduced density state of any quantum spin chains with Z_2 (parity) symmetry [53]. Moreover, Bell-diagonal states contain pure and mixed states, which can be easily prepared in the currently available experimental setups [54–57].

B. The common nonequilibrium dephasing environment

In this subsection, we consider the case where the particle A and quantum memory B are coupled to a common nonequilibrium dephasing environment with non-Markovian and nonstationary features. The total Hamiltonian is given by

$$H = \frac{\hbar}{2}\big[(\omega_0 + \delta(t))\big(\sigma_A^z + \sigma_B^z\big)\big], \tag{10}$$

where A and B have the same intrinsic transition frequency ω_0 and are subjected to common stochastic environmental nonequilibrium fluctuations $\delta(t)$. Thus, employing the approach given in Ref. [46], we can obtain the reduced density matrix for the bipartite system under the common bath case as

$$\varrho^C_{AB}(t) = \begin{pmatrix} \varrho^{11}(0) & \varrho^{12}(0))e^{-i\omega_0 t}\gamma(t) & \varrho^{13}(0)e^{-i\omega_0 t}\gamma(t) & \varrho^{14}(0))e^{-i2\omega_0 t}|\gamma(t)|^4 \\ \varrho^{21}(0)e^{i\omega_0 t}\gamma^*(t) & \varrho^{22}(0) & \varrho^{23}(0) & \varrho^{24}(0)e^{-i\omega_0 t}\gamma^*(t) \\ \varrho^{31}(0)e^{i\omega_0 t}\gamma^*(t) & \varrho^{32}(0) & \varrho^{33}(0) & \varrho^{34}(0)e^{-i\omega_0 t}\gamma^*(t) \\ \varrho^{41}(0)e^{i2\omega_0 t}|\gamma(t)|^4 & \varrho^{42}(0)e^{i\omega_0 t}\gamma(t) & \varrho^{43}(0)e^{i\omega_0 t}\gamma(t) & \varrho^{44}(0) \end{pmatrix}, \tag{11}$$

where C refers to the "common environment" and $\gamma(t)$ is defined in Eq. (6). The above Eq. (11) describes the dynamics of a quantum system (consisting of particle A and quantum memory B) subjected to a common nonequilibrium dephasing environment. We again consider that A and B are initially in the Bell-diagonal states given by Eq. (9). It is essential to mention that in the common bath scenario diagonal elements and two off-diagonal elements, $\varrho^{32}(0)$ and $\varrho^{23}(0)$, remain unchanged, while others decrease with time as $\varrho^C_{AB}(t)$ evolves.

III. EUB UNDER THE LOCAL NONEQUILIBRIUM DEPHASING ENVIRONMENTS

In this section, we study the dynamical behaviors of the EUB when A and B are locally and independently in contact with their own nonequilibrium dephasing environments. However, before presenting our main findings, we first revisit some preliminary concepts and known results from the literature that help us to understand the detailed mechanisms governing the EUB. For this purpose, let us introduce the analytical expression of Eq. (2) for the Bell-diagonal states. The set $\{\sigma^j\}$ with $j \in \{1, 2, 3\}$ represents the Pauli observables. We then choose observables $R_1 = \sigma^1$ and $R_2 = \sigma^3$ for the measurements. Thus, the left-hand side of Eq. (2) takes the form [25]

$$U_{\rm E} = H\left(\frac{1+\mu_1}{2}\right) + H\left(\frac{1+\mu_3}{2}\right), \tag{12}$$

where $U_{\rm E}$ shows the entropic uncertainty for the observables σ^1 and σ^3, while $H(\chi) = -\chi \log_2 \chi - (1-\chi)\log_2(1-\chi)$ defines the binary entropy [47]. Furthermore, for the observables σ^1 and σ^3, the complementarity c is always equal to $1/2$. In the case of Bell-diagonal states, where $S(\varrho_B) = 1$, the right-hand side of Eq. (2) becomes

$$B_{\rm EU} = S(\varrho_{AB}) = -\sum_{l=1}^{4} \eta_l \log_2 \eta_l, \tag{13}$$

where $\eta_{1,2} = [1 \pm \mu_1 \pm \mu_2 - \mu_3]/4$ and $\eta_{3,4} = [1 \pm \mu_1 \mp \mu_2 + \mu_3]/4$ are the eigenvalues of $\varrho_{AB}(0)$. Equation (13) characterizes the entropic uncertainty lower bound (denoted by $B_{\rm EU}$) of the uncertainty, given by Eq. (12).

To understand the fundamental reasons behind the increase or decrease in EUB, we introduce the relationship between QD (represented by $D_{\rm Q}$) and the minimal missing information (represented by M) about A after measurements are performed on B. Mathematically, this relationship can be expressed as (detailed derivation is given in Appendix B)

$$B_{\rm EU} = \log_2 \frac{1}{c} + M - D_{\rm Q}, \tag{14}$$

where for the Bell-diagonal states M can be defined as $M = H((1+\xi)/2)$ with $\xi = \max\{\mu_1, \mu_2, \mu_3\}$ [58] and the analytical expression for QD is provided in Appendix B. Equation (14) reflects that the EUB depends not only on QD but also on M. Interestingly, this relationship renders an avenue to control the dynamical behaviors of EUB by governing the competition between M and QD.

As the dephasing noise process preserves the general form of the Bell-diagonal states, thus the evolved correlation parameters can be easily obtained using the approach provided in Ref. [59]. For the case of local baths with the same decoherence factor, i.e., $\gamma_A(t) = \gamma_B(t) = \gamma$, the evolved parameters can be computed from Eqs. (8) and (9), which take the form $\mu_1(t) = \mu_1|\gamma(t)|^2$ and $\mu_2(t) = \mu_2|\gamma(t)|^2$, and due to the dephasing process $\mu_3(t) = \mu_3$ remains constant. It implies that

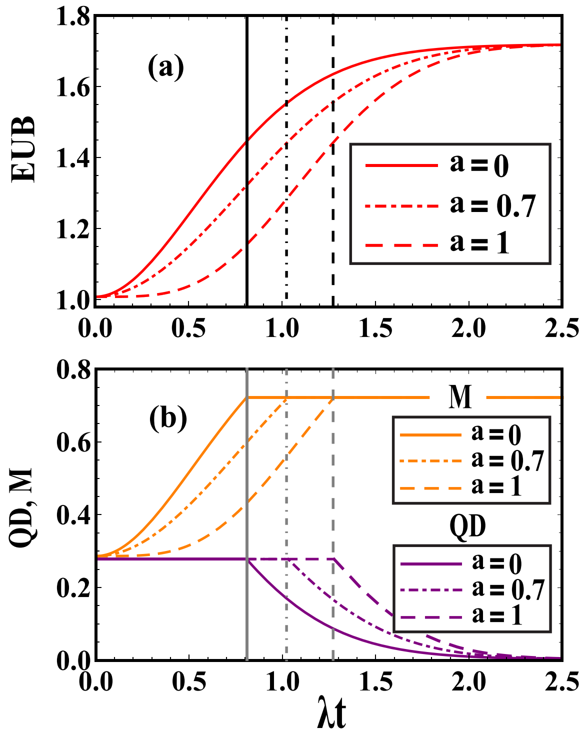

FIG. 1. Dynamics of (a) the entropic uncertainty bound (EUB) (red curves) and (b) quantum discord (QD) (purple curves) and minimal missing information (M) about the measuring particle (orange curves) as a function for timescale λt for different values of a= 0, 0.7, and 1, in the weak-coupling regime with the local baths setup. Here assume the initial-state parameters $\mu_1 = 0.9$, $\mu_2 = 0.54$, $\mu_3 = -0.6$.

these correlation parameters are strongly dependent on the initial value and nature of the dephasing environments. Notably, in our paper, we have set the initial-state parameters as follows: $\mu_1 = 0.9$, $\mu_2 = 0.54$, and $\mu_3 = -0.6$, satisfying the state preparation and measurement choice condition (discussed in Sec. V). Furthermore, these initial-state parameters demonstrate the phenomenon of freezing quantum discord in the case of a local bath setup [37,57]. However, in a common bath scenario, an enhancement in the magnitude of quantum discord towards a steady state can be observed [45] for this initial-state. Interestingly, it will help us unveil the role of these phenomena in the temporal evolution of the EUB. Now, with the assistance of the evolved correlation parameters, we can easily evaluate the dynamics of the entropic uncertainty, entropic uncertainty bound, quantum discord, and minimal missing information about particle A and unveil the effects of the nonequilibrium on them.

In Fig. 1, we plot the time evolution of the EUB, QD, and M when both the measured particle A and quantum memory B are weakly coupled (i.e., $\upsilon/\lambda < 1$; for this case, the dynamics is Markovian [35]) with their respective local nonequilibrium dephasing environments. Particularly, in Fig. 1(a), we display the dynamics of the EUB as a function of the timescale λt for different values of the nonequilibrium parameter a with $\upsilon = 0.8\lambda$, $\beta = \lambda$, and initial correlation parameters $\mu_1 = 0.9$, $\mu_2 = 0.54$, $\mu_3 = -0.6$. When the environment is in equilibrium, i.e., $a = 0$, the magnitude of EUB increases to a stable value, as shown by the red solid curve in Fig. 1(a). The reason behind this increase in EUB can be demonstrated by the competition between the M and QD, as represented by Eq. (14). For $a = 0$, before the vertical gray solid line, one may observe that initially, the quantum discord exhibits a constant value for a certain time interval and then suddenly starts decaying towards zero, while M increases to a steady value, as illustrated by the purple and orange solid curves in Fig. 1(b), respectively. This reflects that the initial enhancement in the magnitude of EUB comes from M because QD stays constant during this period. However, after the vertical black solid line in Fig. 1(a), the increase in the value of EUB is merely due to the decay of QD because M stays constant.

On the other hand, when the environment begins to deviate from equilibrium, for instance, $a = 0.7$, the dephasing in the quantum system reduces [35–37]. As a result, both the time interval for the frozen quantum discord and the time needed for M to reach its maximum significantly increase, as indicated by the position of the vertical gray dot-dashed line in Fig. 1(b). This leads to two remarkable changes in the dynamical behavior of EUB: (i) lowering its value for a specific initial time interval and (ii) slowing the rate at which it tends to maximum value, as illustrated by the red dot-dashed curve in Fig. 1(a). Moreover, we notice a further decrease in the magnitude of the EUB (before reaching a stable value) when dephasing environments move far away from equilibrium, i.e., $a = 1$, as depicted by the red dashed curve in Fig. 1(a). It is evident that this decrease in EUB is caused by the extended duration of the frozen discord and the increased time for M to stabilize when the environment is far from equilibrium ($a = 1$), as displayed by the position of the vertical gray dashed line in Fig. 1(b). These results reveal that the nonequilibrium trait of the dephasing environment offers an alternative and effective avenue to control the time evolution EUB.

Now, we consider the case of the strong-coupling regime (i.e., $\upsilon/\lambda > 1$, indicating non-Markovian dynamics [35]) in Fig. 2, where the EUB exhibits more complex dynamical behaviors that may not be evident in the weak-coupling case. Specifically, in Fig. 2(a), we assume the same initial-state parameters and display the time evolution of EUB for distinct values of a with $\upsilon = 3\lambda$ and $\beta = \lambda$. When the environment is in equilibrium, i.e., $a = 0$, the EUB monotonically increases to a maximal value and then starts oscillations due to the non-Markovianity effect induced by strong-coupling, as illustrated by the red solid curve in Fig. 2(a). According to the relation given by Eq. (14), the initial increase in EUB stems from M because quantum discord remains constant during this initial period, as illustrated by the orange and purple solid curves before the vertical gray solid line in Fig. 2(b), respectively. However, after the vertical gray solid line in Fig. 2(b), only QD starts revivals from zero due to the environmental back-action (non-Markovianity), which is responsible for the oscillations in EUB. On the other hand, when the environment gradually deviates from equilibrium, for example, $a = 0.7$, two significant changes in the dynamics of the EUB can be noticed: a reduction in its magnitude and suppression in the number of oscillations with time, as shown by the red dot-dashed curve in Fig. 2(a). The reason behind these changes in the evolution of EUB can be explained by the competition between QD and M, as mentioned below.

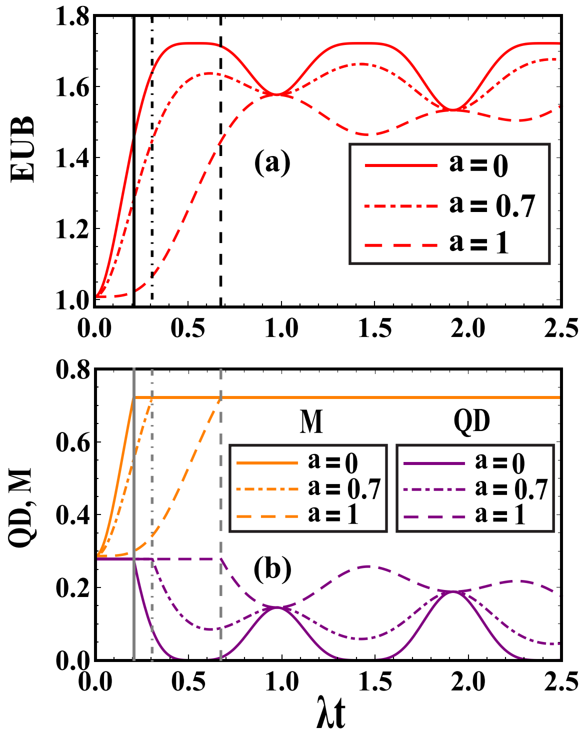

FIG. 2. Dynamics of (a) the entropic uncertainty bound (EUB) (red curves) and (b) quantum discord (QD) (purple curves) and minimal missing information (M) about the measuring particle (orange curves) as a function for timescale λt for different values of $a = 0$, 0.7, and 1, in the strong-coupling regime with the local baths setup. Here assume the initial-state parameters $\mu_1 = 0.9$, $\mu_2 = 0.54$, $\mu_3 = -0.6$.

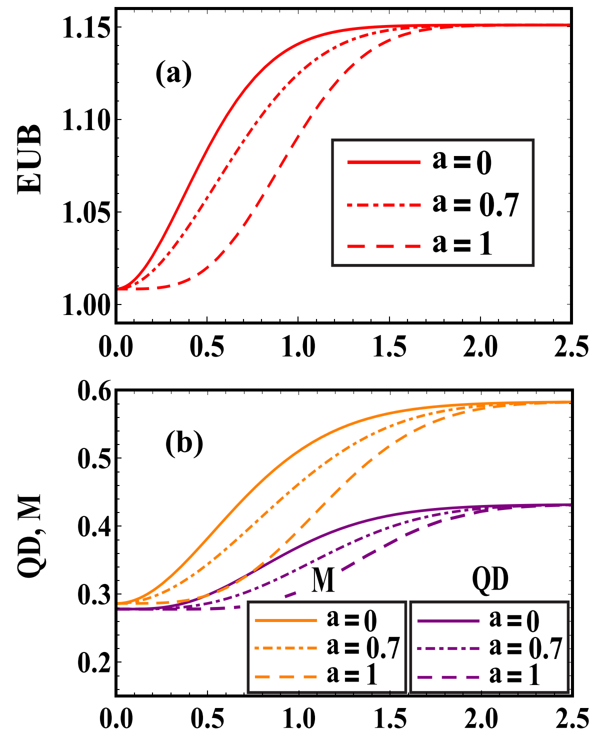

FIG. 3. Dynamics of (a) the entropic uncertainty bound (EUB) (red curves) and (b) quantum discord (QD) (purple curves) and minimal missing information (M) about the measuring particle (orange curves) as a function for timescale λt for different values of $a = 0$, 0.7, and 1, in the weak-coupling regime with a common bath setup. Here assume the initial-state parameters $\mu_1 = 0.9$, $\mu_2 = 0.54$, $\mu_3 = -0.6$.

For $a = 0.7$, the time interval for the frozen QD and the time required for M to achieve its maximum value increase, as indicated by the position of the vertical gray dot-dashed line in Fig. 2(b). Consequently, it leads to a slower rate of rise in the value of EUB, as represented by the red dot-dashed curve in Fig. 2(a). However, when the environment deviates from equilibrium (e.g., $a = 0.7$), QD begins revivals from a nonvanishing value, while M remains time invariant after the vertical gray dot-dashed line throughout the dynamics, as shown in Fig. 2(b). In this scenario, it is evident that nonequilibrium suppresses the non-Markovian effect but intriguingly preserves the QD for a long time, as reported in our earlier studies [37]. It implies that the reduction in the value and the suppression in the number of oscillations of EUB with time are solely due to QD. Moreover, when environments move far away from equilibrium ($a = 1$), one can see more enhancement in the time interval for the frozen QD and the time needed for M to attain its maximum value, as illustrated by the position of the vertical gray dashed line in Fig. 2(b). Additionally, we find that a significant amount of QD can be maintained for an extended period despite the decrease in the amplitudes of the revivals (i.e., environmental back-action) after the vertical gray dashed in Fig. 2(b) when $a = 1$. These dynamical behaviors of M and QD bring remarkable changes in EUB dynamics: (i) a further decrease in the rate of approaching the maximal value, (ii) a decrease in its magnitude, and (iii) a further reduction in the number of oscillations, as depicted by the red dashed curve in Fig. 2(a). It confirms that the nonequilibrium nature of the environments offers a promising protocol to reduce the EUB, though it suppresses the non-Markovian effects. However, we find that the maximum value of EUB (i.e., 1.72) remains the same in both weak- and strong-coupling regimes.

IV. EUB UNDER A COMMON NONEQUILIBRIUM DEPHASING ENVIRONMENT

In this section, we explore the dynamical behaviors of the EUB when both A and B interact with a common nonequilibrium dephasing environment. The evolved correlation parameters under this common environment setup can easily be obtained from Eqs. (9) and (11), which take the form $\mu_1(t) = \frac{1}{2}\{\mu_1[1 + |\gamma(t)|^4] + \mu_2[1 - |\gamma(t)|^4]\}$ and $\mu_2(t) = \frac{1}{2}\{\mu_1[1 - |\gamma(t)|^4] + \mu_2[1 + |\gamma(t)|^4]\}$, and due to the dephasing process $\mu_3(t)$ remains unchanged, i.e., $\mu_3(t) = \mu_3$. With the help of these evolved correlation parameters, we can straightforwardly derive the general dynamical patterns of the EUB, QD, and M.

In contrast to the local baths scenario, the common bath setup renders a promising platform for enhancing and trapping quantum correlations in a steady state [44,45]. Therefore, it would be interesting to ask the following question: Does the EUB reduce when particle A and quantum memory B are coupled with a single common bath? To answer this question, in Fig. 3(a), we plot the dynamics of EUB under the common

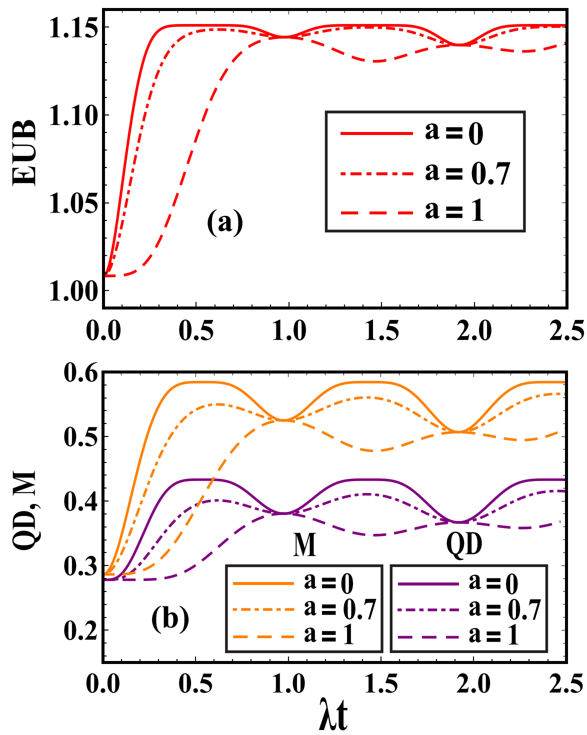

FIG. 4. Dynamics of (a) the entropic uncertainty bound (EUB) (red curves) and (b) quantum discord (QD) (purple curves) and minimal missing information (M) about the measuring particle (orange curves) as a function for timescale λt for different values of $a = 0$, 0.7, and 1, in the strong-coupling regime with a common bath setup. Here assume the initial-state parameters $\mu_1 = 0.9$, $\mu_2 = 0.54$, $\mu_3 = -0.6$.

nonequilibrium dephasing environment, considering the same initial condition and weak-coupling regime, as assumed in Fig. 1(a). Indeed, in Fig. 3(a), we can see that EUB monotonically increases to a stable constant value even though the magnitude of quantum correlations (measured by QD) is enhanced. This increase in EUB can be explained by the relation given in Eq. (14), implying that EUB depends not only on QD but also on M. Therefore, in Fig. 3(b), we illustrate that the common bath setup not only enhances the value of QD but also increases the amount of M simultaneously, contributing to the rise in the value of EUB. Remarkably, however, the maximum value of EUB is significantly lower in the common bath setup (approximately 1.15, while in the case of local baths it is 1.72), as evident from the comparison between Figs. 1 and 3. This difference is due to the increase in the magnitude of QD from its initial value and the suppression of the maximum value of M at the same time in the common bath. Furthermore, similar to the case of the local baths, here the value of EUB also reduces for a specific initial time when the environment deviates from equilibrium, for example, $a = 0.7$ and 1, as shown by the red dot-dashed and dashed curves in Fig. 3(a), respectively.

Next, in Fig. 4, we illustrate the dynamics of EUB, QD, and M in the strong-coupling region, assuming the same initial-state parameters, i.e., $\mu_1 = 0.9$, $\mu_2 = 0.54$, $\mu_3 = -0.6$. Particularly, for $a = 0$, we see that EUB abruptly increases to a maximum value and then begins oscillating from an almost steady state due to the non-Markovianity induced by strong-coupling, as indicated by the red solid curve in Fig. 4(a). Interestingly, in the strong-coupling regime, we also noticed that the maximum value of the EUB is lower in the common bath case than in the local baths setup, as illustrated by comparing Figs. 2(a) and 4(a). According to Eq. (14), in the common bath scenario, the oscillations in the EUB arise remarkably due to the contributions of the revivals in both QD and M, as depicted by the purple and orange solid curves in Fig. 4(b), respectively. However, in the local baths case, the oscillations in the EUB occur solely due to the revivals in QD, as shown in Fig. 2. Furthermore, the reduction in the maximum value of EUB in the common bath is because of the enhancement in amount of QD and the decrease in the maximal value of M. Moreover, the nonequilibrium nature suppresses the amplitude of revivals in both QD and M, as displayed by the purple and orange [$a = 0.7$ dot-dashed; $a = 1$ dashed] curves in Fig. 4(b), respectively. This leads to a reduction in the rate at which EUB tends to maximal value and suppresses its oscillation amplitude as well, as indicated by the red dot-dashed ($a = 0.7$) and dashed ($a = 1$) curves in Fig. 4(a). It can be concluded that the common bath setup offers a promising strategy to reduce the maximum value of EUB in both weak- and strong-coupling regimes, while the nonequilibrium feature of the environment further contributes to its control. Notably, the maximal value (1.15) of EUB remains the same in both coupling regimes.

V. SPMC CONDITION IN LOCAL BATHS AND COMMON BATH SETUPS

In this section, we investigate the state preparation and measurement choice condition under two different nonequilibrium dephasing environmental setups. To this aim, in our paper we choose observables σ^1 and σ^3 for the measurements process. Now if the initial Bell-diagonal state satisfies the condition

$$\mu_2 = -\mu_1\mu_3, \tag{15}$$

then EU $\equiv$ EUB is obeyed in Eq. (2). It implies that the entropic uncertainty in the measurement outcomes of the observables σ^1 and σ^3 can be directly computed via the joint entropy $S(\varrho_{AB})$ of the total system. Equation (15) is referred to as the SPMC condition.

Now, we check the validity of the SPMC condition in both the local baths and common bath cases. For this purpose, we consider that particle A and quantum memory B are in an initial state with $\mu_1 = 0.9$, $\mu_2 = 0.54$, $\mu_3 = -0.6$, which satisfies the SPMC condition. We then first assume that A and B are locally subjected to their respective nonequilibrium dephasing environments. In this situation, the SPMC condition will not be violated, and we can obtain EU $\equiv$ EUB $= S(\varrho_{AB})$ in both weak- and strong-coupling regimes, as illustrated in Figs. 5(a) and 5(b), respectively.

On the other hand, if we consider the same initial-state and bath parameters but assume that both A and B are coupled to a common nonequilibrium dephasing environment, it is observed that the SPMC will not hold in both weak- and strong-coupling cases, as shown in Figs. 6(a) and 6(b), respectively. However, upon comparing Figs. 5 and 6, it becomes

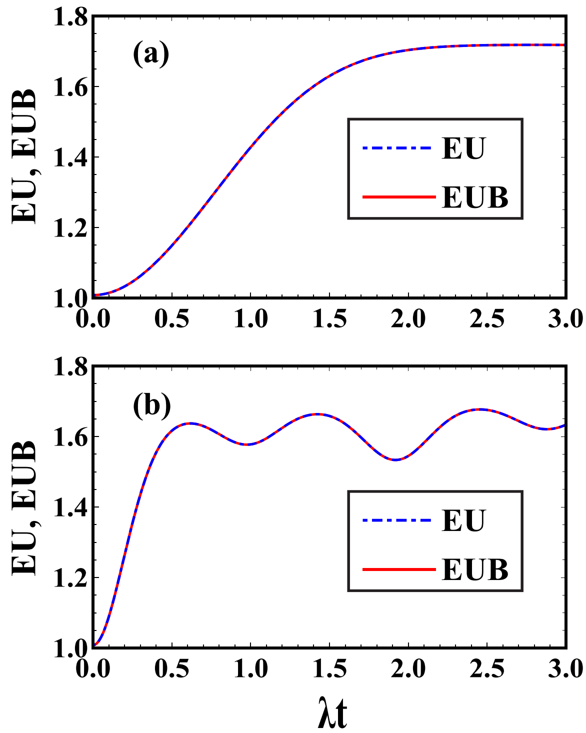

FIG. 5. Dynamics of entropic uncertainty (EU) (blue dot-dashed curves) and the entropic uncertainty bound (EUB) (red solid curves) as a function of timescale λt in (a) weak-coupling and (b) strong-coupling regimes under the local baths setup. Here assume the initial-state parameters $\mu_1 = 0.9$, $\mu_2 = 0.54$, $\mu_3 = -0.6$ with $a = 0.7$.

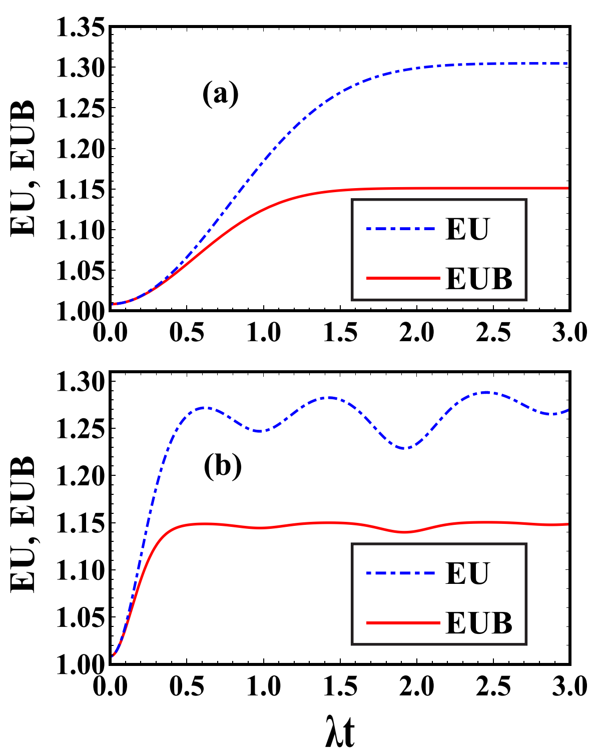

FIG. 6. Dynamics of entropic uncertainty (EU) (blue dot-dashed curves) and the entropic uncertainty bound (EUB) (red solid curves) as a function of timescale λt in (a) weak-coupling and (b) strong-coupling regimes for the common bath case. Here assume the initial-state parameters $\mu_1 = 0.9$, $\mu_2 = 0.54$, $\mu_3 = -0.6$ with $a = 0.7$.

evident that the degree of entropic uncertainty and its lower bound are significantly reduced in the common bath scenario. Furthermore, we reveal that the EUB is not tighter in the common bath; hence, one cannot calculate EU directly from the joint entropy of the whole system.

VI. CONCLUSIONS

We have theoretically investigated the dynamical behaviors of the QMA-EUR for a bipartite system in both local and common nonequilibrium dephasing baths setups. Particularly, we have studied the influence of the competition between nonequilibrium and non-Markovianity in controlling the EUB in weak- and strong-coupling regimes. We have found that the nonequilibrium nature presents a promising approach for efficiently harnessing the EUB in both regimes without demanding any operations on the system of interest. Further, our findings indicate that a common bath can significantly lower the EUB compared to local baths. Moreover, we have clarified the main reasons responsible for governing the dynamical behaviors of EUB by probing the interplay between quantum discord and the minimal missing information about the particle to be measured. In addition, we have analyzed the SPMC condition in both environmental setups with weak- and strong-coupling regimes. Interestingly, we have shown that the SPMC condition does not hold in the common environment scenario for the given initial-state parameters. Therefore, one cannot directly compute the entropic uncertainty from the joint entropy [$S(\varrho_{AB})$] of the total system in the common bath case. Moreover, we intend to expand our current paper and the findings in Ref. [25] to the multipartite system discussed in Refs. [60,61].

ACKNOWLEDGMENTS

The authors wish to thank Dr. X. Cai, A. ur Rahman, and Dr. S. Haddadi for their invaluable discussions during the paper revision.

APPENDIX A: KRAUS OPERATORS OF THE SINGLE AND TWO QUBITS SYSTEMS

The Kraus operators [41,43] for particle A are given by

$$E_A^1(t) = \begin{pmatrix} 1 & 0 \\ 0 & e^{i\omega_0 t}\gamma_A(t) \end{pmatrix},$$
$$E_A^2(t) = \begin{pmatrix} 0 & 0 \\ 0 & \sqrt{1-|\gamma_A(t)|^2} \end{pmatrix}. \quad \text{(A1)}$$

Now, the Kraus operators for the composite system AB, under the local nonequilibrium dephasing environments case, can be simply expressed by the tensor products of each subsystem's Kraus operators [41,43] as follows:

$$F^1(t) = \begin{pmatrix} 1 & 0 \\ 0 & e^{i\omega_0 t}\gamma_A(t) \end{pmatrix} \otimes \begin{pmatrix} 1 & 0 \\ 0 & e^{i\omega_0 t}\gamma_B(t) \end{pmatrix},$$
$$F^2(t) = \begin{pmatrix} 1 & 0 \\ 0 & e^{i\omega_0 t}\gamma_A(t) \end{pmatrix} \otimes \begin{pmatrix} 0 & 0 \\ 0 & \sqrt{1-|\gamma_B(t)|^2} \end{pmatrix},$$

$$F^3(t) = \begin{pmatrix} 0 & 0 \\ 0 & \sqrt{1-|\gamma_A(t)|^2} \end{pmatrix} \otimes \begin{pmatrix} 1 & 0 \\ 0 & e^{i\omega_0 t}\gamma_B(t) \end{pmatrix},$$
$$F^4(t) = \begin{pmatrix} 0 & 0 \\ 0 & \sqrt{1-|\gamma_A(t)|^2} \end{pmatrix} \otimes \begin{pmatrix} 1 & 0 \\ 0 & \sqrt{1-|\gamma_B(t)|^2} \end{pmatrix}. \tag{A2}$$

Here, $\gamma_A(t)$ and $\gamma_B(t)$ are decoherence factors for particle A and quantum memory B, respectively. Further, we consider that both A and B have the same dephasing factor, $\gamma_A(t) = \gamma_B(t) = \gamma(t)$.

APPENDIX B: RELATIONSHIP BETWEEN QD AND EUB

We explore the relationship between QD and the EUB, given by Eq. (2). For this purpose, we recall the definition of QD, i.e.,

$$D_{\mathrm{Q}} = -S(A|B) + \min\{B_i\}\sum_i q_i S\big(\varrho_A^i\big), \tag{B1}$$

where $\min\{B_i\}\sum_i q_i S(\varrho_A^i)$ represents the minimal missing information (which is labeled as M) related to A, given that a set of measurements $\{B_i\}$ is performed on subsystem B [62] and $\varrho_A^i = \frac{tr_B[B_i\varrho_{AB}B_i^\dagger]}{q_i}$ with $q_i = \mathrm{tr}[B_i\varrho_{AB}B_i^\dagger]$. Now Eq. (B1) can be expressed as follows:

$$S(A|B) = M - D_{\mathrm{Q}}. \tag{B2}$$

Thus, from Eqs. (2) and (B2), we can derive the relationship among EUB, QD, and M as given by Eq. (14). Moreover, for the Bell-diagonal states, QD has an analytical expression which is given by [57,58]

$$D_{\mathrm{Q}} = 2 + \sum_{l=1}^{4} \eta_l \log_2 \eta_l - \mathcal{C}, \tag{B3}$$

where $\mathcal{C} = \sum_{i=1}^{2} \frac{1+(-1)^i\xi}{2}\log_2[1+(-1)^i\xi]$, with $\xi = \max\{|\mu_1||\mu_2|,|\mu_3|\}$, characterizes the classical correlations for the bipartite system.

[1] W. Heisenberg, Z. Phys. **43**, 172 (1927).
[2] E. H. Kennard, Z. Phys. **44**, 326 (1927).
[3] H. P. Robertson, Phys. Rev. **34**, 163 (1929).
[4] R. Prevedel, D. R. Hamel, R. Colbeck, K. Fisher, and K. J. Resch, Nat. Phys. **7**, 757 (2011).
[5] I. Białynicki-Birula and J. Mycielski, Commun. Math. Phys. **44**, 129 (1975).
[6] D. Deutsch, Phys. Rev. Lett. **50**, 631 (1983); K. Kraus, Phys. Rev. D **35**, 3070 (1987).
[7] H. Maassen and J. B. M. Uffink, Phys. Rev. Lett. **60**, 1103 (1988).
[8] Y.-K. Kim and Y. Shih, Found. Phys. **29**, 1849 (1999); H. F. Hofmann and S. Takeuchi, Phys. Rev. A **68**, 032103 (2003).
[9] M. Berta, M. Christandl, R. Colbeck, J. M. Renes, and R. Renner, Nat. Phys. **6**, 659 (2010).
[10] I. Devetak and A. Winter, Proc. R. Soc. A **461**, 207 (2005).
[11] C.-F. Li, J.-S. Xu, X.-Y. Xu, K. Li, and G.-C. Guo, Nat. Phys. **7**, 752 (2011).
[12] B. Bergh and M. Garttner, Phys. Rev. Lett. **126**, 190503 (2021).
[13] G. Zhu, A. Liu, L. Xiao, K. Wang, D. Qu, J. Li, C. Qiao, and P. Xue, Phys. Rev. A **108**, L050202 (2023).
[14] M.-L. Hu and H. Fan, Phys. Rev. A **108**, 012423 (2023); P. J. Coles and M. Piani, *ibid.* **89**, 010302(R) (2014); R. Liu, H.-M. Zou, J. Yang, and D. Lin, J. Opt. Soc. Am. B **38**, 662 (2021); Z.-Y. Xu, S.-Q. Zhu, and W.-L. Yang, Appl. Phys. Lett. **101**, 244105 (2012).
[15] T. Pramanik, P. Chowdhury, and A. S. Majumdar, Phys. Rev. Lett. **110**, 020402 (2013).
[16] V. Giovannetti, S. Lloyd, and L. Maccone, Nat. Photon. **5**, 222 (2011).
[17] M.-L. Hu and H. Fan, Phys. Rev. A **86**, 032338 (2012); Y.-H. Sun and Y.-X. Xie, Results Phys. **37**, 105526 (2022).
[18] M. L. Song, L. J. Li, X. K. Song, L. Ye, and D. Wang, Phys. Rev. E **106**, 054107 (2022).
[19] P. J. Coles, M. Berta, M. Tomamichel, and S. Wehner, Rev. Mod. Phys. **89**, 015002 (2017).
[20] M.-L. Hu and H. Fan, Phys. Rev. A **88**, 014105 (2013); P. J. Coles and M. Piani, *ibid.* **89**, 022112 (2014); A. K. Pati, M. M. Wilde, A. R. Usha Devi, A. K. Rajagopal, and Sudha, *ibid.* **86**, 042105 (2012).
[21] F. Adabi, S. Salimi, and S. Haseli, Phys. Rev. A **93**, 062123 (2016); X. Yuan, G. Bai, T. Peng, and X. Ma, *ibid.* **96**, 032313 (2017); Z. Chen, Z. Ma, Y. Xiao, and S.-M. Fei, **98**, 042305 (2018).
[22] F. Ming, D. Wang, X.-G. Fan, W.-N. Shi, Liu Ye, and J.-L. Chen, Phys. Rev. A **102**, 012206 (2020); H. Dolatkhah, S. Haseli, S. Salimi, and A. S. Khorashad, *ibid.* **102**, 052227 (2020); B.-F. Xie, F. Ming, D. Wang, L. Ye, and J.-L. Chen, *ibid.* **104**, 062204 (2021).
[23] L. Wu, L. Ye, and D. Wang, Phys. Rev. A **106**, 062219 (2022); Q.-H. Zhang and S.-M. Fei, *ibid.* **108**, 012211 (2023).
[24] W. H. Zurek, Rev. Mod. Phys. **75**, 715 (2003); L. Aolita, F. de Melo, and L. Davidovich, Rep. Prog. Phys. **78**, 042001 (2015); A. Basit, H. Ali, M. Qurban, F. Badshah, Q. He, and G.-Q. Ge, Phys. Scr. **94**, 125103 (2019); A. Basit, H. Ali, F. Badshah, H. Zhang, R. Ud Din, and G.-Q. Ge, Laser Phys. Lett. **15**, 115204 (2018); A. Basit, F. Badshah, H. Ali, and G.-Q. Ge, Europhys. Lett. **118**, 30002 (2017); A. Basit, H. Ali, F. Badshah, H. Zhang, and G.-Q. Ge, Laser Phys. Lett. **14**, 125202 (2017).
[25] Z. Y. Xu, W. L. Yang, and M. Feng, Phys. Rev. A **86**, 012113 (2012).
[26] M.-L. Hu and H. Fan, Phys. Rev. A **87**, 022314 (2013).
[27] G. Karpat, J. Piilo, and S. Maniscalco, Europhys. Lett. **111**, 50006 (2015); G. Karpat, Can. J. Phys. **96**, 700 (2018).
[28] D. Wang, F. Ming, M.-L. Hu, and L. Ye, Ann. Phys. (Leipzig) **531**, 1900124 (2019); S. Haseli, Eur. Phys. J. Plus **135**, 761 (2020).
[29] S. Haddadi, S. Haseli, M. R. Pourkarimi, and F. Mirmasoudi, Phys. Scr. **96**, 075104 (2021); B. Li, L. Feng, J. Shi, and T. Wu, Laser Phys. Lett. **20**, 025201 (2023).
[30] R. A. Abdelghany, A.-B. A. Mohamed, M. Tammam, W. Kuo, and H. Eleuch, Sci. Rep. **11**, 11830 (2021); A. N. Khedr, A.-B. A. Mohamed, A.-H. Abdel-Aty, M. Tammam, M. Abdel-Aty, and H. Eleuch, Entropy **23**, 1595 (2021).

[31] A.-B. A. Mohamed, F. M. Aldosari, S. M. Younis, and H. Eleuch, Chaos Solit. Fractals **177**, 114213 (2023); A. H. Abdel-Aty, A.-B. A. Mohamed, A. U. Rahman, and H. Eleuch, Fractals **30**, 2240185 (2022).
[32] M.-N. Chen, W.-Y. Sun, A.-J. Huang, F. Ming, D. Wang, and L. Ye, Laser Phys. Lett. **15**, 015207 (2018); F. Ming, D. Wang, A.-J. Huang, W.-Y. Sun, and L. Ye, Quantum Inf. Process. **17**, 9 (2018).
[33] Y.-B. Yao, D. Wang, F. Ming, and L. Ye, J. Phys. B **53**, 035501 (2020); J. Hu and Q. Xue, Chin. Phys. B **28**, 070303 (2019).
[34] M.-N. Chen, D. Wang, and Liu Ye, Phys. Lett. A **383**, 977 (2019); G.-Q. Zhang and J.-B. Xu, J. Opt. Soc. Am. B **36**, 205 (2019).
[35] X. Cai and Y. Zheng, Phys. Rev. A **94**, 042110 (2016); X. Meng, Y. Sun, Q. Wang, J. Ren, and X. Cai, Entropy **25**, 634 (2023).
[36] X. Cai and Y. Zheng, J. Chem. Phys. **149**, 094107 (2018); X. Cai, R. Meng, Y. Zheng, and L. Wang, Europhys. Lett. **125**, 30007 (2019).
[37] A. Basit, H. Ali, F. Badshah, X.-F. Yang, and G.-.Q. Ge, New J. Phys. **22**, 033039 (2020); Phys. Rev. A **104**, 042417 (2021); A. Basit, H. Ali, X.-F. Yang, and G. Ge, Phys. Scr. **96**, 075105 (2021).
[38] X. Cai and Y. Zheng, Phys. Rev. A **95**, 052104 (2017).
[39] D. Lin, H.-M. Zou, and J. Yang, Phys. Scr. **95**, 015103 (2020).
[40] W. W. Cheng, Ann. Phys. (Leipzig) **535**, 2300180 (2023).
[41] H. Chen, T. Han, M. Chen, J. Ren, X. Cai, X. Meng, and Y. Peng, Photonics **10**, 134 (2023).
[42] W. W. Cheng and B. Li, Quantum Inf. Process. **22**, 294 (2023).
[43] M. Chen, H. Chen, T. Han, and X. Cai, Entropy **24**, 1330 (2022).
[44] A. Basit, H. Ali, P.-B. Li, and G. Xianlong, Phys. Rev. A **107**, 042432 (2023); J.-B. Yuan, L.-M. Kuang, and J.-Q. Liao, J. Phys. B **43**, 165503 (2010).
[45] J.-S. Zhang and A.-X. Chen, J. Phys. B **47**, 215502 (2014).
[46] T. Yu and J. H. Eberly, Phys. Rev. B **68**, 165322 (2003); K. Ann and G. Jaeger, *ibid.* **75**, 115307 (2007); T. Yu and J. H. Eberly, Phys. Rev. Lett. **93**, 140404 (2004); B. Bellomo, R. Lo Franco, and G. Compagno, *ibid.* **99**, 160502 (2007).
[47] M. A. Nielsen and I. L. Chuang, *Quantum Computation and Quantum Information* (Cambridge University, Cambridge, England, 2000).
[48] H. P. Breuer and F. Petruccione, *The Theory of Open Quantum Systems* (Oxford University, New York, 2002); A. Basit, H. Ali, F. Badshah, and G.-Q. Ge, Commun. Theor. Phys. **68**, 29 (2017).
[49] P. W. Anderson, J. Phys. Soc. Jpn. **9**, 316 (1954).
[50] R. Kubo, J. Phys. Soc. Jpn. **9**, 935 (1954).
[51] M. Ban, S. Kitajima, and F. Shibata, Phys. Rev. A **82**, 022111 (2010).
[52] R. Kubo, M. Toda, and N. Hashitsume, *Statistical Physics II: Nonequilibrium Statistical Mechanics* (Springer-Verlag, Berlin, 1985).
[53] M. S. Sarandy, T. R. de Oliveira, and L. Amico, Int. J. Mod. Phys. B **27**, 1345030 (2013).
[54] R. Auccaise, L. C. Céleri, D. O. Soares-Pinto, E. R. deAzevedo, J. Maziero, A. M. Souza, T. J. Bonagamba, R. S. Sarthour, I. S. Oliveira, and R. M. Serra, Phys. Rev. Lett. **107**, 140403 (2011).
[55] X. Rong, F. Jin, Z. Wang, J. Geng, C. Ju, Y. Wang, R. Zhang, C. Duan, M. Shi, and J. Du, Phys. Rev. B **88**, 054419 (2013); A. Basit, H. Ali, F. Badshah, X.-F. Yang, and G.-Q. Ge, Laser Phys. Lett. **18**, 065202 (2021).
[56] F. M. Paula, I. A. Silva, J. D. Montealegre, A. M. Souza, E. R. deAzevedo, R. S. Sarthour, A. Saguia, I. S. Oliveira, D. O. Soares-Pinto, G. Adesso, and M. S. Sarandy, Phys. Rev. Lett. **111**, 250401 (2013).
[57] I. A. Silva, A. M. Souza, T. R. Bromley, M. Cianciaruso, R. Marx, Roberto S. Sarthour, I. S. Oliveira, R. Lo Franco, S. J. Glaser, E. R. deAzevedo, D. O. Soares-Pinto, and G. Adesso, Phys. Rev. Lett. **117**, 160402 (2016); L. Mazzola, J. Piilo, and S. Maniscalco, *ibid.* **104**, 200401 (2010).
[58] S. Luo, Phys. Rev. A **77**, 042303 (2008).
[59] P. C. Obando, F. M. Paula, and M. S. Sarandy, Phys. Rev. A **92**, 032307 (2015).
[60] S. Liu, L.-Z. Mu, and H. Fan, Phys. Rev. A **91**, 042133 (2015).
[61] S. Haddadi, M. R. Pourkarimi, and S. Haseli, Sci. Rep. **11**, 13752 (2021).
[62] H. Ollivier and W. H. Zurek, Phys. Rev. Lett. **88**, 017901 (2001); L. Henderson and V. Vedral, J. Phys. A **34**, 6899 (2001).